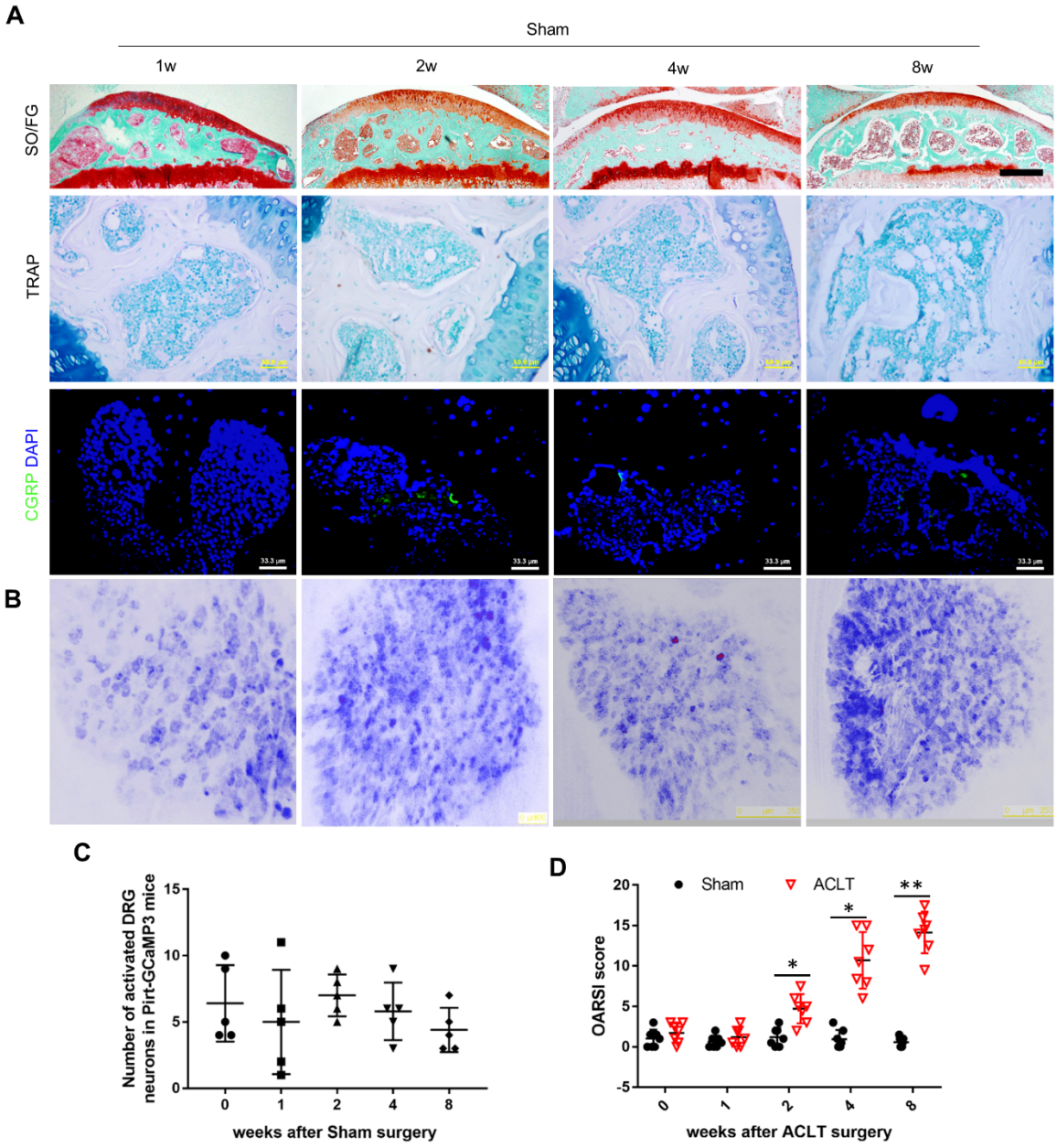

Supplementary Figure 1 (A) Safranin orange staining (top), TRAP staining (2nd row, magenta), and immunofluorescent analysis of CGRP^{+} sensory nerve fibers (3rd row, green) in mouse tibial subchondral bone after sham surgery at different time points. Scale bars, 500 μm (top), 100 μm (2nd row), 50 μm (3rd row). **(B)** Excitability (bottom) of L4 DRG in *Pirt-GCaMP3* mice at different time points after sham surgery. Scale bar, 100 μm. (See full videos of neuronal hyperactivity in supplementary materials). **(C)** Quantification of lit up DRG neurons in *Pirt-GCaMP3* mice at different time points after sham surgery. **(D)** OARSI scores of both ACLT

and sham-operated mice at different time points. *p < 0.05, **p < 0.01 compared with the sham-operated group at the corresponding time points. *n* = 7 per group.

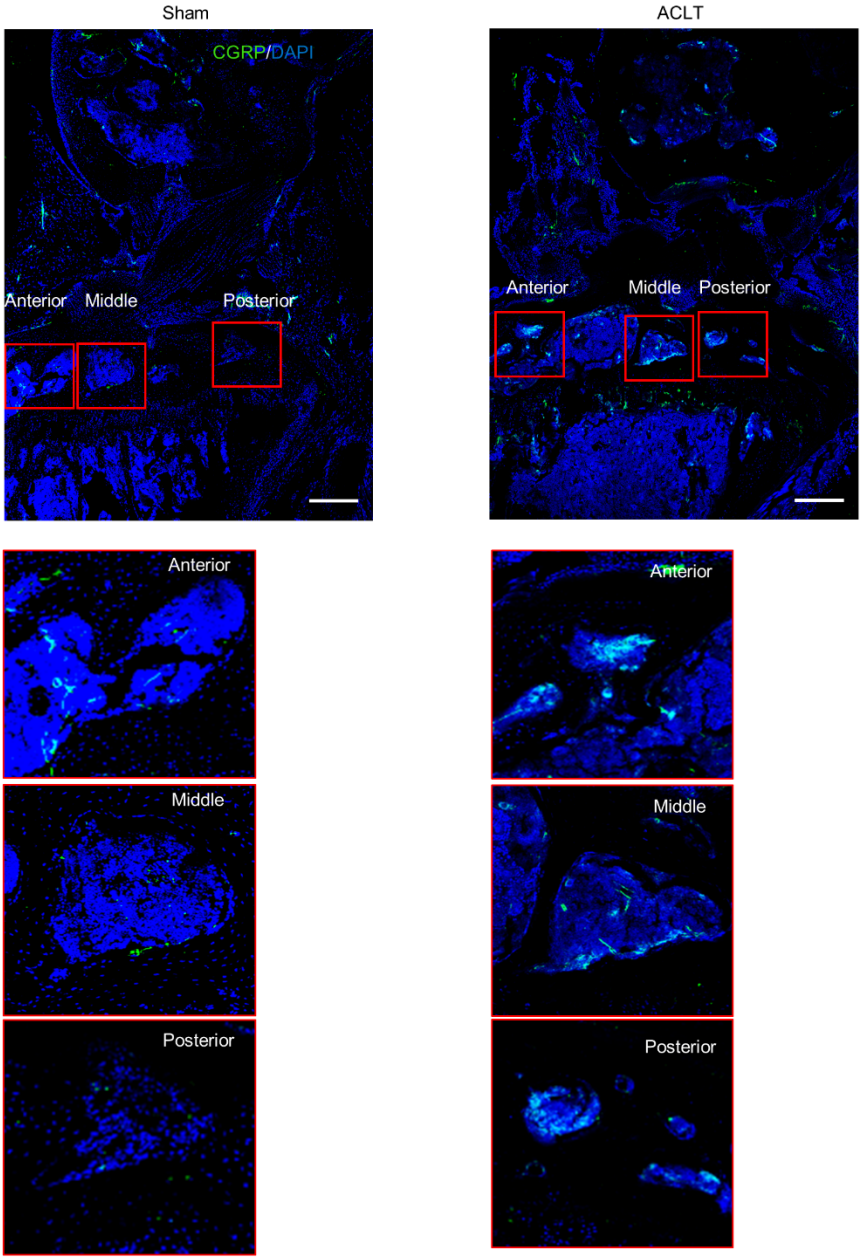

Supplementary Figure 2 Overviews of the mouse knee stained with CGRP. Left, an overview of sham group mice knee section stained with CGRP. Red boxes indicate higher magnification pictures taken in anterior, middle, and posterior areas of tibial subchondral bone. Right, an overview of ACLT group mice knee section stained with CGRP. Scale bar, 500 μm.

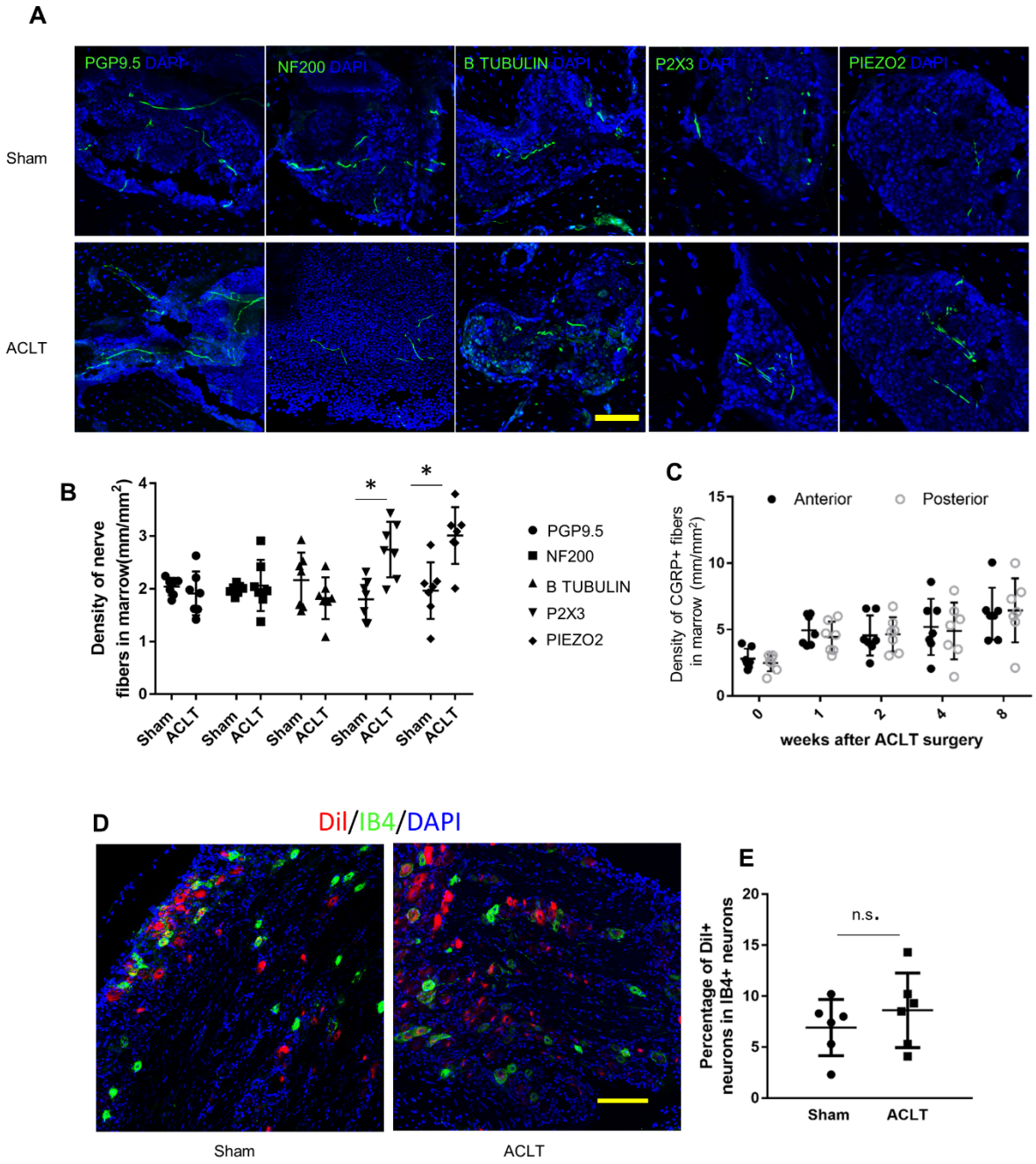

Supplementary Figure 3 (A) Immunofluorescent staining of PGP9.5 (1st column), NF200 (2nd column), B TUBULIN (3rd column), P2X3 (4th column), and PIEZO2 (5th column) in the subchondral bone of sham and ACLT operated mice. Scale bar, 50 μm. **(B)** Quantification of density of PGP9.5, NF200, B TUBULIN, P2X3, and PIEZO2 in the subchondral bone of sham and ACLT operated mice. **(C)** Quantification of $CGRP^+$ sensory nerves density in tibial subchondral bone divided by posterior and anterior area. (**D)** Representative photomicrographs of IB4 and Dil double-labeled neurons in L4 DRG. Scale bar, 50 μm. **(E)** Percentage of L4 DRG

IB4+ neurons retrogradely labeled Dil in all IB4+ neurons 10 weeks after sham or ACLT surgery.

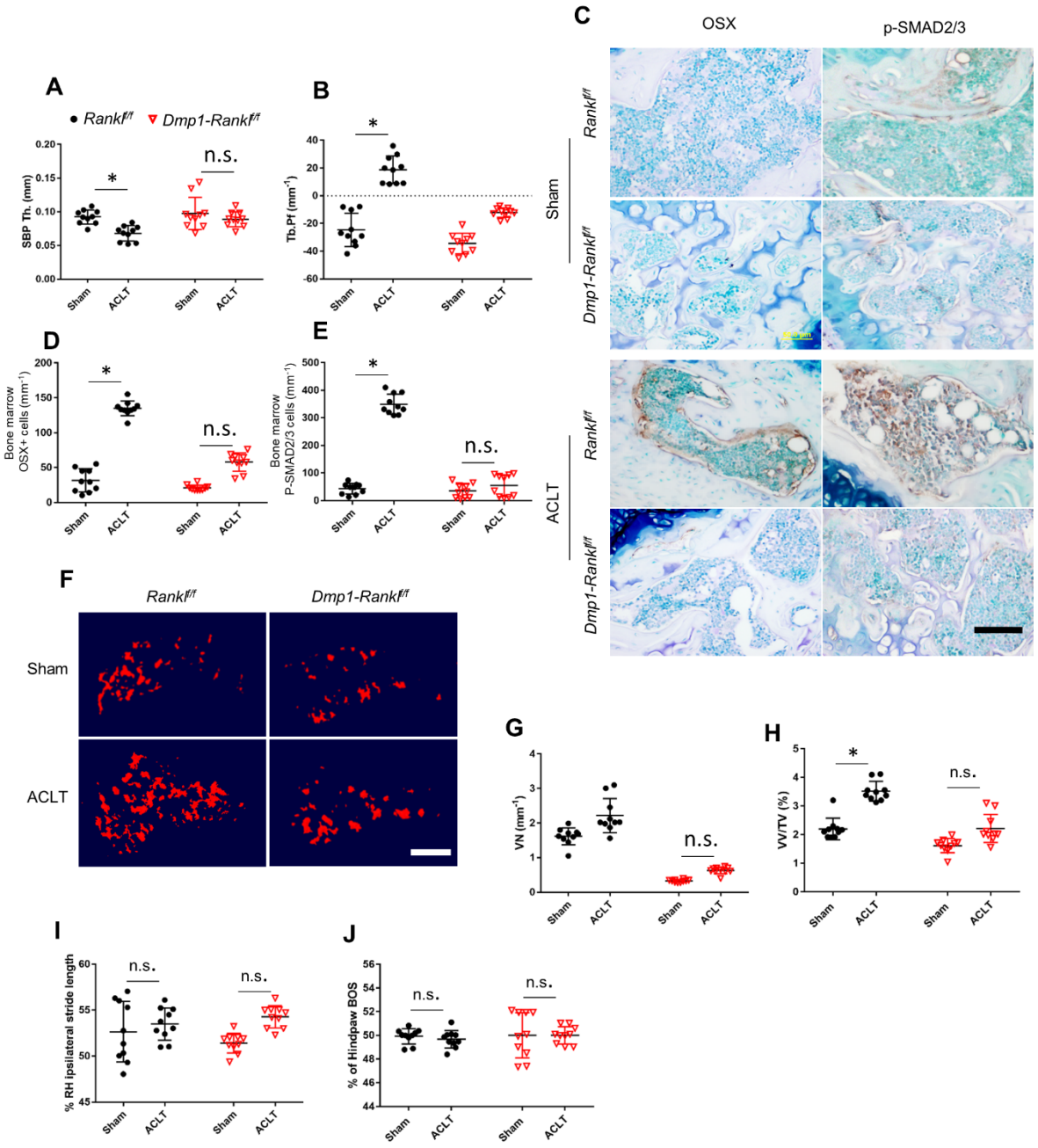

Supplementary Figure 4 Subchondral bone properties and gait analysis of quantitative analysis of *Rankl*$^{f/f}$ and *Dmp1-Rankl*$^{f/f}$ mice. **(A,B)** Thickness of SBPs (SBP Th.) **(A)** and trabecular pattern factor (Tb.Pf.) **(B)** in subchondral bone determined by µCT analysis 8 weeks after ACLT surgery. $n = 10$ per group. *$p < 0.05$, n.s. = no significant difference. **(C)** Immunohistochemistry of OSTERIX and p-SMAD2/3 in subchondral bone of *Rankl*$^{f/f}$ and *Dmp1-Rankl*$^{f/f}$ with or without

ACLT surgery. **(D,E)** Quantifications of bone marrow OSX+ and p-SMAD2/3+ cells. *p < 0.05, n.s. = no significant difference. **(F)** CT-based microangiogram of the tibial subchondral bone of *Rankl*$^{f/f}$ and *Dmp1-Rankl*$^{f/f}$ with or without ACLT surgery. Scale bar, 500 μm. **(G,H)** Quantification of vessel volume relative to tissue volume (VV/TV) and vessel number (VN). *n* = 10 per group. *p < 0.05, n.s. = no significant difference. **(I,J)** Quantitative analysis of percentage RH ipsilateral stride length **(I)** and percentage hind paw base of support **(J)** were measured and calculated using Image J software. *n* = 10 per group. n.s. = no significant difference.

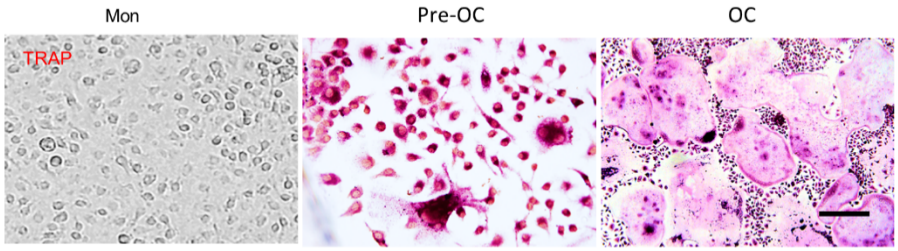

Supplementary Figure 5 TRAP staining of monocytes (Mon) (left), pre-osteoclasts (Pre-OC) (middle), and osteoclasts (OC) (right). Scale bar, 100 μm.

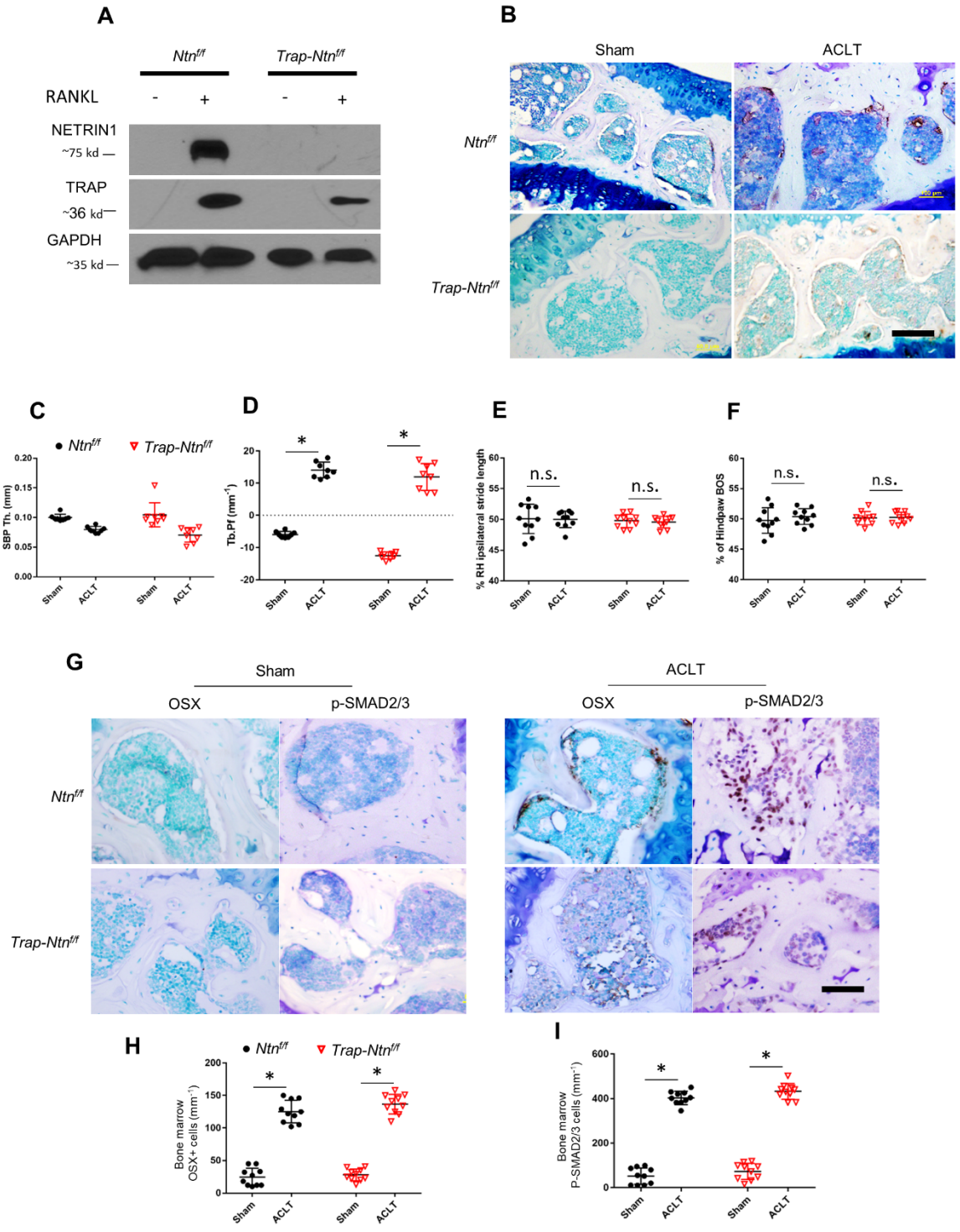

Supplementary Figure 6 Deletion of netrin-1 in subchondral bone osteoclasts of *Trap-Nnt$^{f/f}$* mice did not affect subchondral bone remodeling. **(A)** Western blot analysis of netrin-1 deletion in osteoclasts in *Trap-Nnt$^{f/f}$*. **(B)** Immunohistochemistry of netrin-1 in subchondral bone of *Nnt$^{f/f}$*

and *Trap-Nnt*$^{f/f}$ mice with or without ACLT. Scale bar, 50 μm. **(C,D)** Quantitative analysis of thickness of SBPs (SBP Th.) **(C)** and Tb.Pf **(D)** in subchondral bone determined by μCT analysis. n = 8 per group. **(E,F)** Quantitative analysis of percentage RH ipsilateral stride length **(E)** and percentage hind paw base of support **(F)** were measured and calculated using Image J software. n = 10 per group. **(G)** Immunohistochemistry of OSX and p-SMAD2/3 in subchondral bone of *Nnt*$^{f/f}$ and *Trap-Nnt*$^{f/f}$ with or without ACLT surgery. **(H,I)** Quantifications of bone marrow OSX+ and p-SMAD2/3+ cells. *p < 0.05. Statistical significance was determined by multifactorial ANOVA, and all data are shown as means ± standard deviations.

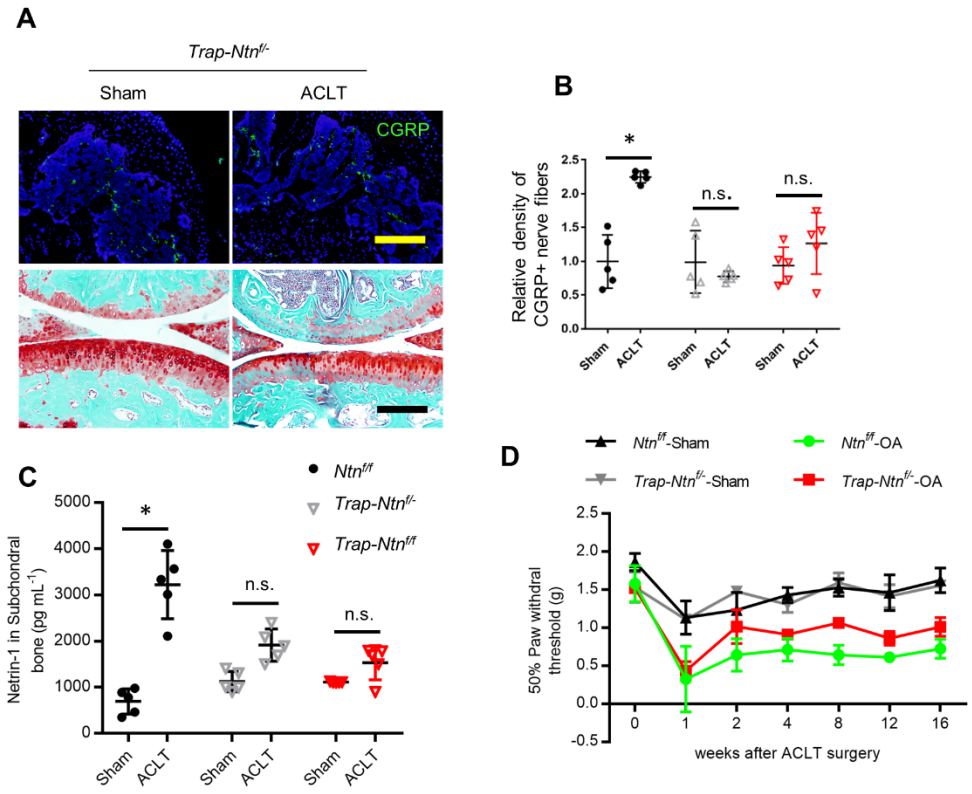

Supplementary Figure 7 Decreased CGRP+ sensory nerves in *Trap-Nnt*$^{f/-}$ subchondral bone. **(A)** Immunofluorescence analysis of CGRP+ sensory nerve fibers in mouse tibial subchondral bone after ACLT surgery. Scale bars, 50 μm. **(B)** Quantitative analysis of relative pixel ratio of CGRP+ length to total bone surface. *p < 0.05, n.s. = no significant difference. **(C)** ELISA analysis of netrin-1 concentration in subchondral bone marrow of *Nnt*$^{f/f}$, *Trap-Nnt*$^{f/f}$, and *Trap-Nnt*$^{f/-}$ mice with or without ACLT surgery. *p < 0.05, n.s., no significant difference. Statistical significance was determined by multifactorial ANOVA, and all data are shown as means ±

standard deviations. **(D)** Paw withdrawal threshold (PWT) was tested at the right hindpaw of *Nnt*$^{f/f}$-sham, *Nnt*$^{f/f}$-ACLT, *Trap*- *Nnt*$^{f/-}$-sham, and *Trap*- *Nnt*$^{f/-}$-ACLT mice.

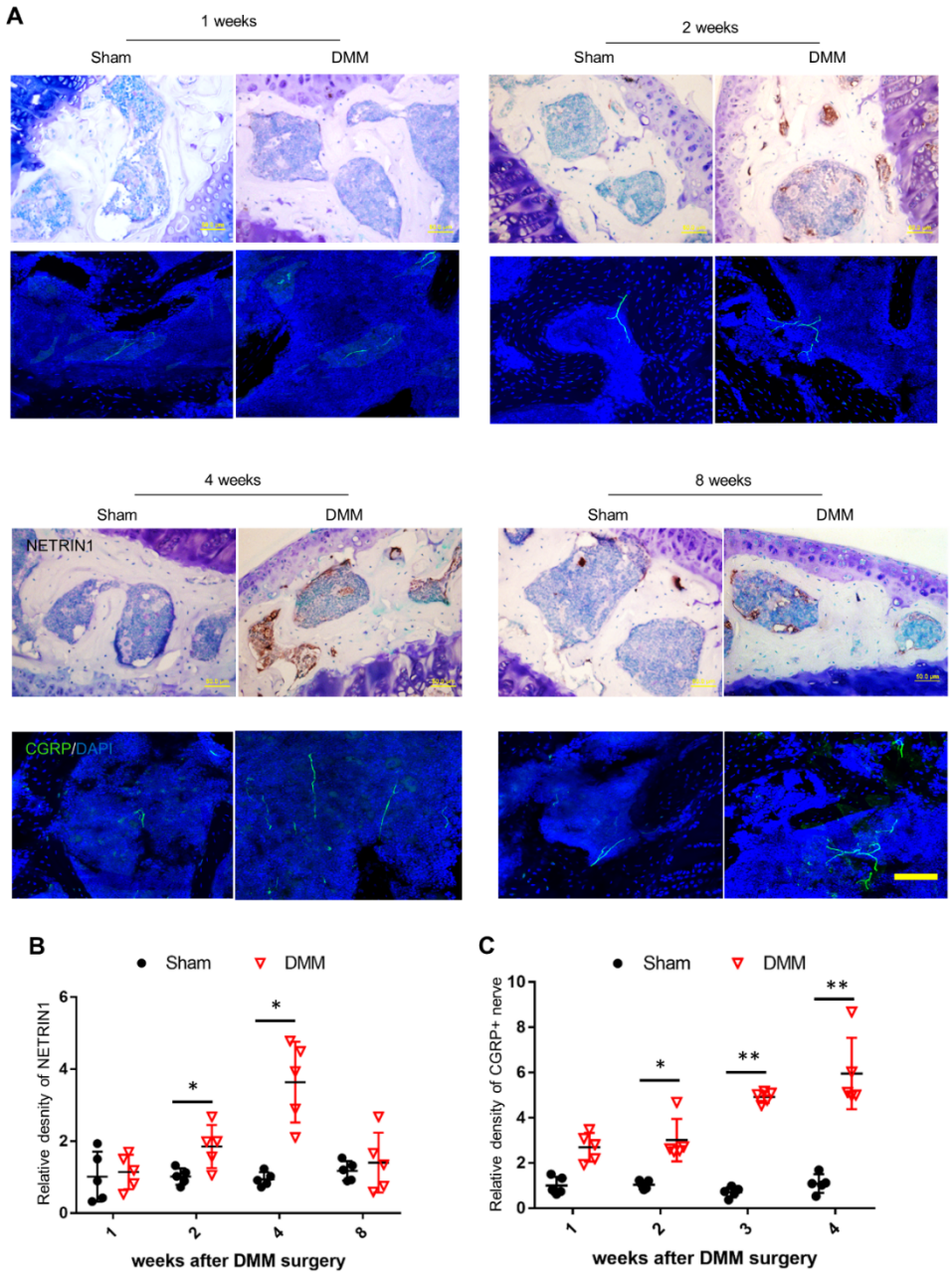

Supplementary Figure 8 Increased subchondral bone CGRP^{+} sensory nerves and netrin-1 in subchondral bone of DMM mice. **(A)** Immunohistochemical staining of netrin-1 (top row) and immunofluorescent staining of CGRP (bottom row) in subchondral bone of sham and DMM operated mice at 1, 2, 4, and 8 weeks. Scale bars, 50 μm. **(B)** Quantification of relative density of netrin-1 staining in subchondral bone of DMM mice at different time points. *p < 0.05. **(C)**

Quantification of relative CGRP+ nerve fiber density in subchondral bone of DMM mice at different time points. *p < 0.05, **p < 0.01. Statistical significance was determined by multifactorial ANOVA, and all data are shown as means ± standard deviations.

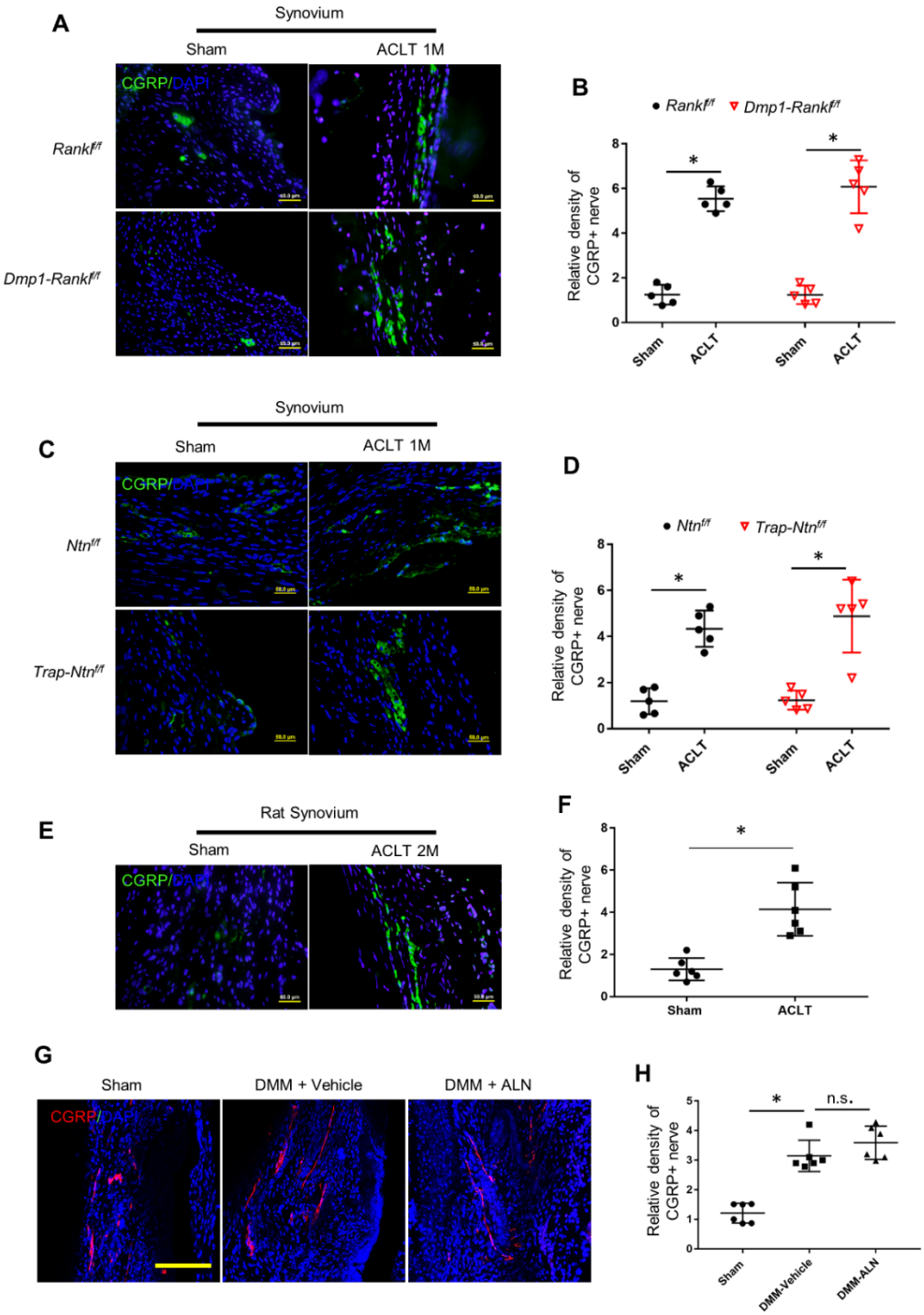

Supplementary Figure 9 CGRP+ nerve fibers increased after ACLT in synovium of both *Dmp1-Rankl*$^{f/f}$ mice and *Trap-Nnt*$^{f/f}$ mice. **(A)** Immunofluorescent staining of CGRP in synovium of *Rankl*$^{f/f}$ and *Dmp1-Rankl*$^{f/f}$ mice with or without ACLT. Scale bars, 50 μm. **(B)** Quantification of relative CGRP+ nerve fibers density in synovium of sham and ACLT mice. *p < 0.05. **(C)** Immunofluorescent staining of CGRP in synovium of *Nnt*$^{f/f}$ and *Trap-Nnt*$^{f/f}$ mice with or without ACLT. Scale bars, 50 μm. **(D)** Quantification of relative CGRP+ nerve fiber density in synovium of sham and ACLT mice. *p < 0.05. **(E)** Immunofluorescent staining of CGRP in synovium of rats with or without ACLT. Scale bars, 50 μm. **(F)** Quantification of relative CGRP+ nerve fiber density in rat synovium. *p < 0.05. **(G)** Immunofluorescent staining of CGRP in synovium of mice treated with vehicle or alendronate. Scale bars, 50 μm. **(H)** Quantification of relative CGRP+ nerve fiber density in synovium of mice treated with vehicle or alendronate. *p < 0.05. n.s., no significant difference.

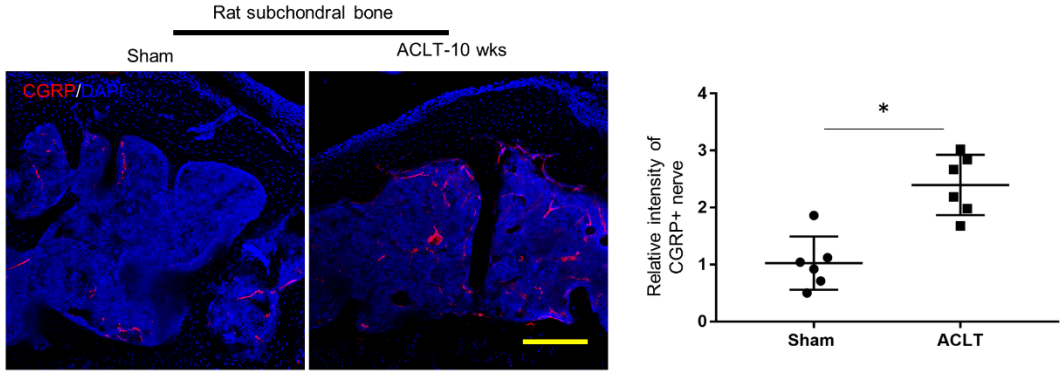

Supplementary Figure 10 (A) Immunofluorescent staining of CGRP+ sensory nerve fibers in subchondral bone of rat 10 weeks after ACLT. **(B)** Quantification of relative CGRP^{+} nerve fiber density in subchondral bone of rat with or without ACLT. *p < 0.05. Scale bar, 50 μm.

Supplementary information of methods

Mice

We obtained the *Trap-Cre* mouse strain from Dr. J. J. Windle (Virginia Commonwealth University, Richmond, VA, USA). We obtained the *netrin-1*$^{f/f}$ mouse strain from Dr. H. K. Eltzschig (The University of Texas Health Science Center at Houston, Houston, TX, USA). We purchased the *Dmp1-Cre* and *Rankl*$^{f/f}$ mouse strains from the Jackson Laboratory (Bar Harbor, ME, USA). *Pirt-GCaMP3* mice were obtained from Dr. Xinzhong Dong (The Johns Hopkins School of Medicine, Baltimore, MD, USA). Briefly, *Pirt-GCaMP3* mice were generated by targeted homologous recombination to replace the entire coding region of the *Pirt* gene (phosphoinositide interacting regulator of transient receptor potential channels) gene with the GCaMP3 sequence fused with a neomycin resistance gene sequence and put in-frame with the Pirt promoter. *Pirt-GCaMP3* heterozygotes were used in all experiments.

Hemizygous *Trap-Cre* mice were crossed with *netrin-1*$^{f/f}$ mice. The offspring were intercrossed to generate the following offspring: WT mice, *Trap-Cre* mice (expressing Cre recombinase driven by *Tra*p promoter), *netrin-1*$^{flox/flox}$ mice (homozygous for *netrin-1* flox allele), and *Trap-Cre*;*netrin-1*$^{f/f}$ mice (with *netrin-1* conditional deletion in *Trap* lineage cells). *Trap-Cre;netrin-1*$^{f/f}$ or *netrin-1*$^{f/f}$ mice were further crossed with *Pirt-GCaMP3* mice to yield *Trap-Nnt*$^{f-}$*;Pirt-GCaMP3* mice. Because Pirt and netrin-1 are located at the same chromosome (chromosome 11, NC_000077.6) and applying for the law of linkage and crossing-over, we could obtain only *Trap- Nnt*$^{f/-}$*; Pirt-GCaMP3* mice.

Hemizygous *Dmp1-Cre* mice were crossed with *Rankl*$^{f/f}$ mice. The offspring were intercrossed to generate the following offspring: WT mice, *Dmp1-Cre* mice (expressing Cre recombinase driven by *Dmp1* promoter), *Rankl*$^{f/f}$ mice (homozygous for *RANKL* flox allele), and *Dmp1-Rankl*$^{f/f}$ mice (with *RANKL* conditional deletion in *Dmp1* lineage cells). *Dmp1-Rankl*$^{f/f}$ or *Rankl*$^{f/f}$ mice were further crossed with *Pirt-GCaMP3* mice to yield *Dmp1-Rankl*$^{f/f}$*;Pirt-GCaMP3* mice and *Rankl*$^{f/f}$*;Pirt-GCaMP3* mice.

We determined the genotypes of the mice by polymerase chain reaction analyses of genomic DNA isolated from mouse tails using the following primers:
Trap-Cre forward, 5′-ATATCTCACGTACTGACGGTGGG-3′ and reverse, 5′-CTGTTTCACTATCCAGGTTACGG-3′; flox *Ntn* allele forward, 5′-AGGTAAAGTCTCCTACGCGG-3′ and reverse, 5′-CTTCCAAACCTGAACCGCCC-3′;

Dmp1-Cre, forward, 5′-CCCGCAGAACCTGAAGATG-3′ and reverse, 5′-GACCCGGCAAAACAGGTAG-3′; flox *Rankl*, forward, 5′-CTGGGAGCGCAGGTTAAATA-3′, reverse 5′- GCCAATAATTAAAATACTGCAGGAAA-3′ Pirt-GCaMP3 primer1, 5′-TCCCCTCTACTGAGAGCCAG-3′, primer 2, 5′-GGCCCTATCATCCTGAGCAC-3′ and primer3, 5′-ATAGCTCTGACTGCGTGACC-3′.

Histochemistry, immunohistochemistry, and histomorphometry

At the time of euthanasia, we resected and fixed the mouse knee joints in 10% buffered formalin for 48 h, decalcified them in 10% ethylenediaminetetraacetic acid (EDTA, pH 7.4) for 14 d, and embedded them in paraffin or optimal cutting temperature compound (Sakura Finetek). Four-μm-thick sagittal-oriented sections of the knee joint medial compartment were processed for hematoxylin and eosin, safranin orange, and fast green staining. Tartrate-resistant acid phosphatase (TRAP) staining was performed using a standard protocol (Sigma-Aldrich). For immunohistology, slides were incubated with antigen retrieval buffer (ab208572, Abcam) at 100 ˚C for 1 h, cooled to room temperature, and washed with tris-buffered saline (TBS). For immunohistochemistry, the sections were incubated with 0.3% H_2O_2 in tris-buffered saline for 15 min, then blocked with 1X phosphate-buffered saline (PBS)/5% normal serum/0.3% Triton X-100 (Dow Chemical Company) for 1 h. We incubated sections with primary antibodies to mouse osterix (1:600, ab22552, Abcam), pSmad2/3 (1:50, sc-11769, Santa Cruz Biotechnology), netrin-1 (sc-20786, H-104, Santa Cruz Biotechnology), TRAP (1:200, Polyclonal, Santa Cruz Biotechnology), CGRP (1:200, ab81887, Abcam), PGP9.5 (1:100, ab10404, Abcam), DCC (1:100, ab201260, Abcam), and NF-200 (1:100, ab8135, Abcam) overnight at 4 °C. For immunohistochemical staining, a horseradish peroxidase–streptavidin detection system (Dako, Agilent Technologies) was used to detect immunoactivity, followed by counterstaining with ethyl green (Sigma-Aldrich). For immunofluorescence staining, secondary antibodies conjugated with fluorescence (Alexa Fluor 488 or 546) were added, and slides were incubated at room temperature for 1 h while avoiding light. We microphotographed sections (DP71 microscope camera, Olympus) to perform histomorphometric measurements on the entire area of the tibial subchondral bone. Quantitative histomorphometric analysis was conducted in a blinded fashion using OsteoMeasureXP software (Osteometrics). We counted the number of positively stained cells in the whole tibial subchondral bone area per specimen in 5 sequential sections per mouse

in each group. We calculated OARSI scores as described previously(86). The whole knee joints paraffin blocks were subjected to serial ~4-μm sagittal sections through the medial compartment. 4 or 5 sections were collected on each slide.

Synovial CGRP staining

The joint sections were sectioned and picked as aforementioned. The stained sections were initially scanned at low magnification (x100) to identify areas of synovium. 5 confocal images (x400) of sections separated by ~20-μm were obtained. The obtained images were then analyzed with Imag-Pro v.6.0, and nerve fibers were manually traced to determine their respective lengths. The area of synovium was also manually traced to determine area. Then the data were reported as density of nerve fibers of synovium (mm/mm^2).

High-resolution μCT

We dissected mouse knee joints free of soft tissue, fixed them overnight in 70% ethanol, and analyzed them using high-resolution μCT (SkyScan 1172, Bruker microCT). We reconstructed and analyzed images using NRecon v1.6, and CTAn v1.9, respectively. Three-dimensional model visualization software, CTVol v2.0 (Bruker microCT), was used to analyze parameters of the trabecular bone in the epiphysis. The scanner was set at a voltage of 50 kVp, a current of 200 μA, and a resolution of 5.7 μM per pixel. Sagittal images of the tibial subchondral bone were used to perform 3-dimensional histomorphometric analyses. We defined the region of interest to cover the whole subchondral bone medial compartment, and we used 8 consecutive images from the medial tibial plateau for 3-dimensional reconstruction and analysis. Three-dimensional structural parameters analyzed included the following: TV (total tissue volume; containing both trabecular and cortical bone), BV/TV (trabecular bone volume per tissue volume), Tb.Th (trabecular thickness), Tb.Sp (trabecular separation), SMI (structure model index), Conn.Dn (connectivity density) and Tb.Pf (trabecular pattern factor). Tb.Pf was first developed and described by Hahn and colleagues(87) to quantify the connectedness of trabecular plates. Their concept is that the connectedness of structures can be described by the relation of convex to concave surfaces. Many concave surfaces represent a well-connected spongy lattice, and many

convex surfaces indicate a poorly connected trabecular lattice, which is an indication of early changes in trabecular bone structure.

Preparation of conditioned media from preosteoclasts and osteoclasts

We prepared different types of conditioned media from preosteoclasts or osteoclasts. We harvested monocytes and macrophages from bone marrow of 6-week-old WT male mice by flushing the marrow space of femora and tibiae. We cultured the flushed bone marrow cells overnight on Petri dishes in α-minimum essential medium (MEM) containing 10% fetal bovine serum, 100 U ml^{-1} penicillin, 100 μg ml^{-1}streptomycin sulfate, and 30 ng/ml^{-1} macrophage colony-stimulating factor (M-CSF) (R&D Systems). After discarding the adherent cells, we incubated floating cells with M-CSF (30 ng/ml) to obtain pure monocytes and macrophages. Upon incubation of monocytes and macrophages in 24-well plates (1×10^5 cells per well) with 30 ng/ml M-CSF and 60 ng/ml RANKL (PeproTech), nearly all cells became preosteoclasts after a 3-d culture. Alternatively, fully mature multinucleated osteoclasts were formed after incubation with 30 ng/ml M-CSF and 200 ng/ml RANKL for 8 d. We detected TRAP activities of the cultured preosteoclasts and mature osteoclasts using a commercial kit (Sigma-Aldrich). At the end of induction, we harvested serum-containing conditioned media from the preosteoclasts and mature osteoclasts. After centrifugation (2,500 r.p.m. for 10 min at 4 °C), we aliquoted conditioned media and stored it at −80 °C.

DRG neuron culture

To prepare the DRG neuron culture medium, MEM was supplemented with 5% fetal bovine serum (Gibco), 1X penicillin-streptomycin solution (500 units of penicillin and 500 μg of streptomycin, Gibco), 1X GlutaMAX-I supplement (35050-061, Thermo Fisher Scientific), and the antimitotic reagents containing 20 μM 5-fluoro-2-deoxyuridine (F0503, Sigma-Aldrich) and 20 μM uridine (U3003, Sigma-Aldrich). Lumbar DRGs were dissected and harvested from 8-week-old mice. DRG neurons were digested and dissociated with 1 ml collagenase A solution (10103578001, Roche) and incubated at 37 ˚C for 90 min followed by 500 μl 1X TrypLE Express solution (15140-122, Thermo Fisher Scientific) at 37 ˚C for 30 min. TrypLE Express solution was removed, and DRG were washed 3 times with 1 ml prepared culture medium (containing 5% fetal bovine serum). Tissue was triturated by adding 600 μl culture medium and

gently pipetting up and down 20–30 times. After trituration, non-dissociated tissues were allowed to settle to the bottom of the microfuge, and the DRG neuron suspension was transferred to another tube.

Microfluidics assay

Corning No. 1 cover glasses (24 × 40 mm) and Standard Neuron Device (450-μm microgroove barrier, SND450) were placed on a suitable tray with face feature side up in plasma cleaner (PIE Scientific). The device and cover glasses were exposed to the plasma for 2 min. Under a clean fume hood, the neuron device was placed on the cover glass and pressed down evenly to ensure bonding. The device was coated with 100 μg/ml Poly-D-Lysine (P6407, Sigma-Aldrich) and 10 μg/ml Laminin (23017-015, Invitrogen) in an incubator at 37 ºC for 4 h according to manufacturer's instructions. The device was washed 5 times with dH_2O. DRG neurons were loaded at a concentration of 2.5 to 4.5 million cells per ml in 1 well (50,000 to 90,000 cells) on the left side of the neuron device. Loading of neurons was verified under a microscope to ensure the neurons were flowing into the device's main channel. The device containing neurons was incubated at 37 ºC in a 5% CO_2 incubator for 10 min to allow the cells to attach. Approximately 150 μl of culture medium was added to each top well, allowing the media to flow through the device for 30 s to 1 min before filling the bottom wells with media. Conditioned media (150 μl) from monocytes, preosteoclasts, and osteoclasts with or without antibodies (Slit3, 1 μg/ml [AF3629, R&D Systems]; netrin-1, 1 μg/ml [MAB1109, R&D Systems]; ephrin B2, 1 μg/ml [MABN482, EMD Millipore]; SEMA3A, 1 μg/ml [ab23393, Abcam]) or mouse recombinant netrin-1 peptide, 200 ng/ml (AAC52971, R&D Systems) was added to each well on the right side. The device was incubated for 2 d. The DRG neurons and their nerve fibers were subjected to standard immunofluorescence staining. Briefly, 150 μl of 100% methanol (chilled at –20 ºC) was added at room temperature for 5 min, followed by 4% paraformaldehyde in PBS (pH 7.4) for 10 min at room temperature. Cells were incubated for 10 min with PBS containing 0.25% Triton X-100. Cells were washed 3 times in PBS for 5 min. Cells were blocked with 1% bovine serum albumin for 30 min, then incubated in diluted Alexia Fluor 488 Phalloidin (Thermo Fisher Scientific) at room temperature for 1 h. The solution was decanted, and cells were washed 3 times in PBS for 5 min. Nerve fibers that crossed the microchannels were microphotographed

using an Olympus DP71 camera. The length of nerve fibers that crossed the microchannels was quantified using ImageJ software.

Von Frey test

Von Frey hair algesiometry was used to measure the 50% PWT. Mice were placed in elevated Plexiglas chambers (30 cm long × 9 cm wide × 24 cm tall) on metal mesh flooring, which allows access to the plantar surface of the paws. After allowing the animal to acclimate until exploratory behavior ceased (~20 min), ipsilateral hind paw mechano-sensitivity was assessed using a modification of the Dixon up-down method(51, 86). A von Frey hair of known bending force (force range ≈ 0.07 g, 0.4 g, 0.6 g, 1 g, 1.4 g, 2 g, 4 g, or 6 g) was applied perpendicular to the plantar surface of the hind paw (avoiding the toe pads) until it just bent, and then was held in place for 2–3 s. If there was no response, the next higher strength hair was applied up to a maximum level that corresponded to a 6-g bending force. After the first difference in response was observed, 4 more measurements were made. The 50% PWT was determined using the following formula: $10^{[Xf + k\delta]}$ / 10,000, where Xf is the value (in log units) of the final von Frey hair used, k is the tabular value for the pattern of the last 6 positive/negative responses, and δ is the mean difference (in log units) between stimuli. The threshold force required to elicit withdrawal of the paw (median 50% withdrawal) was determined twice on each hind paw (and averaged) on each testing day, with sequential measurements separated by at least 5 min.

Ink blot analysis

To provide a consistent length and width to the technique, we conducted ink blot analysis using the tunnel provided with the CatWalk system. The mouse front paws were covered with black ink and the hind paws were covered with orange ink. The drawings of footprints were scanned and imported to ImageJ software for analyzing intensity, contact area, and distance between each paw. All distances were measured in pixels. Distances were measured from the heel of 1 print to the heel of the designated print of interest. “Stride length” was the distance between the same limbs. Percentage of RH ipsilateral stride length was the percentage of ipsilateral RH length to the total length of RH and right front (RF) ipsilateral stride length. BOS was determined by the distance between both front and hind limbs. BOS refers to the area beneath a mouse that includes every point of contact that the paws make with the supporting surface. The BOS is an important concept for understanding an individual’s ability to balance. A wide BOS has long been believed to be a hallmark of unsteady gait in humans(80). Percentage hind paw BOS was the percentage

of hind paw BOS relative to the total BOS of front paws and hind paws. Percentage RH ipsilateral intensity and percentage RH ipsilateral contact area allow visualization of uneven weightbearing distribution or pressure areas. Briefly, the contact area and intensity of each footprint were measured using ImageJ software. Percentage RH ipsilateral intensity and percentage RH ipsilateral contact area were the percentages of RH paw intensity/contact area to the total intensity/contact area of right front and hind paws, respectively.

Parameters measured in CatWalk analysis

1) Paw pressure (light intensity, which is the mean brightness of all pixels of the print at maximum paw contact, ranging from 0–255 arbitrary units). It has been reported that animals with OA minimize contact with the floor and exert less pressure on the painful limb during walking, thus showing decreased weightbearing in the osteoarthritic limb. In the CatWalk test, weightbearing on the 2 hind paws was measured through signal intensity.

2) Paw print area (complete surface area contacted by the paw during the stance phase). One gait cycle is also known as a stride. Each stride has 2 phases: the stance phase, during which the foot remains in contact with the floor, and the swing phase, during which the foot is not in contact with the floor.

3) Stance phase (duration in seconds of contact of a paw with the glass plate during a step cycle [i.e., stance phase + swing phase]).

4) Swing phase (duration in seconds of no paw contact with the glass plate during a step cycle).

5) Duty cycle (stance duration as a percentage of the step cycle duration [i.e., stance phase / (stance + swing phases) × 100]).

6) Stride length (distance between successive placements of the same paw).

7) Swing speed (speed of a paw during the swing phase [i.e., stride length / swing phase duration]).

Western blotting

Western blot analyses were conducted on the protein of lysates from *in vitro* DRG neurons and osteoclasts. The cell lysates were centrifuged, and the supernatants were separated by SDS-PAGE and blotted on a polyvinylidene fluoride membrane (Bio-Rad Laboratories). After incubation in specific antibodies, we detected proteins using an enhanced chemiluminescence kit (Amersham Biosciences). We used antibodies recognizing mouse Akt (1:500, 2920S, Cell

Signaling Technology), p-Akt (Ser 473, Cell Signaling Technology, 1:1,000, 4058S), p-FAK (1:500, Polyclonal, Santa Cruz Biotechnology), FAK (1:500, Polyclonal, Santa Cruz Biotechnology), netrin-1 (ab126729, Abcam), TRAP (1:500, sc-376875, Santa Cruz Biotechnology), and GAPDH (1:1000, sc-365062, Santa Cruz Biotechnology) to examine the protein concentrations in the lysates.

***In vivo* and *in vitro* RNA interference**

In vivo RNA interference was performed using mouse DCC siRNA (4457308; Ambion In Vivo, Thermo Fisher Scientific) and negative control siRNA (4459405, Thermo Fisher Scientific). Before siRNA administration, the siRNA was mixed with Invivofectamine 3.0 (Thermo Fisher Scientific), a liposome-based formulation for better tissue targeting, according to the manufacturer's instructions. Briefly, the siRNA and Invivofectamine 3.0 were mixed and heated at 60 ˚C for 30 min and diluted to the final concentration of 2.5 mg/ml by endotoxin-free PBS (pH 7.4). Intravenous injections were performed through the mouse dorsal tail vein using a 27-gauge needle. The siRNA was injected at a dose of 2 mg/kg every 3 d until the mice were euthanized at 4 weeks after ACLT. For *in vitro* siRNA transfection, siDCC (sc-6535, Santa Cruz Biotechnology) and siUNC5b (sc-67902, Santa Cruz Biotechnology) were transfected into dissected primary mouse DRG neurons according to the manufacturer's guidelines. Briefly, 3 d after neuron seeding, media were replaced and incubated for 24 h for transfection. Lipofectamine RNAi MAX (13778100, Invitrogen) was diluted in OptiMEM (31985062, Thermo Fisher Scientific) and incubated for 5 min, then combined with siRNA and incubated for another 5 min. Diluted DNA and Lipofectamine RNAi MAX were mixed and incubated at room temperature for 20 min and then used to transfect the neurons. The media were replaced 8 h after transfection.

ELISA of netrin-1 in cultured media and subchondral bone

We determined the concentration of NETRIN1 in the conditioned media using the ELISA development kit (EKC37454, Biomatik) according to the manufacturer's instructions. Under a dissecting microscope, we first used forceps to carefully dissociate the tibial subchondral bone cap (separate from the growth plate). We then put the cap into PBS buffer in a 1.5-ml Eppendorf tube (growth plate side facing the tube bottom). Then, high-speed centrifugation (16,000 g, 20 min) was applied to spin out the subchondral bone marrow (red). The bone marrow was then homogenized and used for ELISA analysis.

Retrograde tracing

Three-month-old male Sprague Dawley rats (Charles River Laboratories) (300–400 g, $n = 6$ per group) were used to perform ACLT as previously described(56). At 8 weeks after sham surgery or ACLT, all rats were anesthetized with ketamine and xylazine. A 20-mm parapatellar incision was made over the medial side of the left knee. After adequate exposure of the knee joint, ipsilateral femoral and tibial subchondral bone were subjected to retrograde labeling. We injected 2 μL Dil (Molecular Probes; 5 mg/ml in N, N dimethylformamide) into the femoral and tibial subchondral bone areas using a Hamilton syringe with a 27-gauge needle. Immediately after injection, bone wax was used to seal the drilling holes to prevent tracer leakage. After Dil injection, the wound was sutured, and a heat pad was used to protect animals during recovery from anesthesia. Animals were euthanized 2 weeks after retrograde injection with an overdose of isoflurane inhalation, and the left lumbar DRGs (L4, L5) were isolated for immunofluorescence. Twenty-μm frozen sections were used, and the Dil signals were inspected under 564-nm excitation using a confocal microscope (LSM 780, Zeiss). Twenty sections from each DRG were used for statistical analysis.

DRG exposure surgery for *in vivo* imaging of the whole L4 DRG

For all imaging experiments, mice aged 2 months or older were anesthetized by intraperitoneal injection of ketamine and xylazine. After deep anesthesia was reached, each animal's back was shaved and aseptically prepared, and ophthalmic ointment (Lacrilube; Allergan Pharmaceuticals) was applied to the eyes to prevent drying. During surgery, mice were kept on a heating pad (DC temperature controller, FHC) to maintain body temperature at 37 ºC ± 0.5 ºC as monitored by a rectal probe. Dorsal laminectomy was usually performed at spinal level L6 to S1 below the lumbar enlargement (but occasionally lower than S1) without removing the dura (some experimental conditions, such as direct local drug injection into DRG tissue and rhodamine injection into DRG neurons, required removal of the dura). A 2-cm midline incision was made around the lower part of the lumbar enlargement, and paravertebral muscles were dissected away to expose the lower lumbar part that surrounds the L3–L5 vertebrae. The L4 DRG transverse processes were exposed and cleaned. Using small rongeurs, we removed the surface aspect of the L4 DRG transverse process near the vertebrae (only the L4 DRG transverse process was

removed, but the bone over the spinal cord was intact) to expose the underlying DRG without damaging the DRG or spinal cord. Bleeding from the bone was stopped using styptic cotton.

The videos were analyzed to quantify the changes in calcium signal intensity in response to mechanical force. All cells that were lit up were regarded as a region of interest. Calcium signal changes throughout the recording were displayed as $\Delta F / F_o = (F_t - F_o) / F_o$. F_o = the mean intensity of the region of interest during the baseline period before the mechanical force. F_t was measured throughout the recording.

Stimulus delivery during imaging experiments

Press stimuli were delivered using a rodent pincher analgesia meter, which was pressed to the operative knees of the mice. The mechanical force was controlled manually by the experimenter at approximately 20 g. We determined the force applied to the knee on the basis of a preliminary experiment performed on mice before ACLT surgery. We used a rodent pincher analgesia meter to apply force to the knee and gradually increased the force until 1–10 neurons were activated. A ~20-g force was then chosen and used for other experiments in this study. The duration of the mechanical force was 15–30 s after 40–50 s of baseline imaging.

***In vivo* DRG calcium imaging**

In vivo imaging of the whole L4 DRG in live mice was performed for 1–6 h immediately after surgery. Body temperature was maintained at 37 ºC ± 0.5 ºC on a heating pad while rectal temperature was monitored. After surgery, mice were laid in the abdomen-down position on a custom-designed microscope stage. The spinal column was stabilized using custom-designed clamps to minimize movements caused by breathing and heartbeat. In addition, a custom-designed head holder was used as an anesthesia/gas mask. The animals were maintained under continuous anesthesia for the duration of the imaging experiment with 1%–2% isoflurane gas using a gas vaporizer. Pure oxygen was used to deliver the gas to the animal. The microscope stage was fixed under a laser-scanning confocal microscope (Leica LSI microscope system), which was equipped with a macrobased, large-objective fast EM-CCD camera. Live images were acquired at 8–10 frames with 600 Hz in frame-scan mode per 6–7 s, at depths below the dura ranging from 0–70 μm, using a 5 × 0.5 NA macro dry objective at 512 × 512–pixel resolution with solid diode lasers (Leica Camera) tuned at 488- and 532-nm wavelength and emission at 500–550 nm for green, respectively. For analysis, raw image stacks (512 × 512 to 1024 × 1024

pixels in the x-y plane and 20–30 μm voxel depth; 10 optical sections) were imported into ImageJ software for further analysis. DRG neurons were at the focal plane, and imaging was monitored during the activation of DRG neuron cell bodies by peripheral stimuli. To compare the sizes of responding cells between sham and DMM mice for a particular stimulus, we calculated the areas of the ROIs in Fiji. For each calcium imaging video, a frequency distribution using relative frequencies was calculated for the responding cell areas using a bin range with bin centers from 150–1550 μm^2 and a bin width of 100 μm^2. Areas greater than 800 μm^2 were summed into 1 bin. The calculated relative frequencies for each size category were averaged across the mice for either DMM or sham treatment.